Observational constraint on the radius and oblateness of the lunar core-mantle boundary

Vishnu Viswanathan, Nicolas Rambaux, Agnes Fienga, Jacques Laskar, Mickael Gastineau

▶ **To cite this version:**

Vishnu Viswanathan, Nicolas Rambaux, Agnes Fienga, Jacques Laskar, Mickael Gastineau. Observational constraint on the radius and oblateness of the lunar core-mantle boundary. Geophys.Res.Lett., 2019, 46, pp.7295-7303. 10.1029/2019GL082677 . hal-02088588

HAL Id: hal-02088588
https://hal.science/hal-02088588v1

Submitted on 7 Jan 2022

HAL is a multi-disciplinary open access archive for the deposit and dissemination of scientific research documents, whether they are published or not. The documents may come from teaching and research institutions in France or abroad, or from public or private research centers.

L'archive ouverte pluridisciplinaire **HAL**, est destinée au dépôt et à la diffusion de documents scientifiques de niveau recherche, publiés ou non, émanant des établissements d'enseignement et de recherche français ou étrangers, des laboratoires publics ou privés.

Copyright

Check for updates

AGU100 ADVANCING EARTH AND SPACE SCIENCE

Geophysical Research Letters

RESEARCH LETTER
10.1029/2019GL082677

Special Section:
50 years of Apollo Science

Observational Constraint on the Radius and Oblateness of the Lunar Core-Mantle Boundary

V. Viswanathan[1,2], N. Rambaux[1], A. Fienga[1,2], J. Laskar[1], and M. Gastineau[1]

[1]ASD/IMCCE, CNRS, Observatoire de Paris, PSL Université, Sorbonne Université, Paris, France, [2]AstroGéo/Géoazur, CNRS, Université Côte d'Azur, Observatoire de la Côte d'Azur, Valbonne, France

Key Points:
- LLR and GRAIL gravity field data are used to perform fits of a lunar interior's dynamical model
- Estimates of core oblateness intersect with corresponding theoretical values of a hydrostatic core
- The accuracy of oblateness and radii of a presently relaxed lunar core is improved by a factor of 3

Supporting Information:
- Supporting Information S1

Correspondence to:
V. Viswanathan and N. Rambaux,
vishnu.viswanathan@obspm.fr;
nicolas.rambaux@obspm.fr

Citation:
Viswanathan, V., Rambaux, N., Fienga, A., Laskar, J., & Gastineau, M. (2019). Observational constraint on the radius and oblateness of the lunar core-mantle boundary. *Geophysical Research Letters*, *46*, 7295–7303. https://doi.org/10.1029/2019GL082677

Received 4 MAR 2019
Accepted 19 JUN 2019
Accepted article online 8 JUL 2019
Published online 9 JUL 2019

Abstract Lunar laser ranging (LLR) data and Apollo seismic data analyses, revealed independent evidence for the presence of a fluid lunar core. However, the size of the lunar fluid core remained uncertain by ±55 km (encompassing two contrasting 2011 Apollo seismic data analyses). Here we show that a new description of the lunar interior's dynamical model provides a determination of the radius and geometry of the lunar core-mantle boundary (CMB) from the LLR observations. We compare the present-day lunar core oblateness obtained from LLR analysis with the expected hydrostatic model values, over a range of previously expected CMB radii. The findings suggest a core oblateness ($f_c = (2.2 \pm 0.6) \times 10^{-4}$) that satisfies the assumption of hydrostatic equilibrium over a tight range of lunar CMB radii ($\mathcal{R}_{\mathrm{CMB}} = 381 \pm 12$ km). Our estimates of a presently relaxed lunar CMB translates to a core mass fraction in the range of 1.59–1.77% with a present-day free core nutation within (367 ± 100) years.

Plain Language Summary The study of the rotation of a body gives access to key information about its interior. Using a set of numerically integrated equations, Earth-Moon distance information from lunar laser ranging (LLR) data, and the knowledge of Moon's gravity from the Gravity Recovery and Interior Laboratory mission, we are able to simulate the rotation and motion of the Moon in the vicinity of Earth, Sun, and other planetary bodies with high accuracy. In this study, we compare the expected relaxed shape of the Moon's core with that obtained from a best-fit adjustment of our simulation parameters to the observed LLR data. This novel approach allows us to improve the previous uncertainty in the radius and polar flattening of the Moon's core-mantle boundary (CMB), both by a factor of 3. Limits on the size of the lunar CMB provide significant constraints to important works such as the Earth-Moon formation (e.g., giant impact) hypotheses. In addition, a better constraint on the lunar CMB radii translates to an improvement on the precision tests of fundamental physics using LLR data. Furthermore, our methods can be applied to study the influence of the liquid core on the rotation of other planets, especially Mars, with the recent advent of the InSight mission.

1. Introduction

1.1. State of the Art

Lunar laser ranging (LLR) consists of measuring the round-trip travel time of a laser pulse emitted from an observing station on the Earth and received back after bouncing-off of a retroreflector array on the surface of the Moon. LLR observations to these optical devices on the near side of the Moon (five sites, as a part of the payloads of the NASA Apollo and Russian Lunokhod missions) continue to be collected since 1969 (Bender et al., 1973). The accuracy of these range measurements gradually improved from the initial few tens of centimeters in the 1970s, to a few centimeters in the 1990s, to millimeter-level accuracies since the 2000s (Courde et al., 2017; Murphy, 2013). At present, the entire LLR data set spans 48 years in time, greater than a factor of 2 times the period of lunar nodal precession of 18.6 years. The analyses and results retrieved by using such highly accurate range measurements span multidisciplinary science such as geodesy and geodynamics, solar system ephemerides, terrestrial and celestial reference frames, lunar physics, and fundamental physics (e.g., Dickey et al., 1994; Murphy, 2013).

The lunar science derived from LLR depends on the accurate monitoring of the time-varying lunar orientation and orbital motion. A mathematical description of the orbital and rotational dynamics of the Moon is referred to as the dynamical model. This model includes the mutual interactions between the interior layers of the Moon (i.e., crust/mantle and fluid core) as well as perturbations from other planetary

©2019. American Geophysical Union. All Rights Reserved.

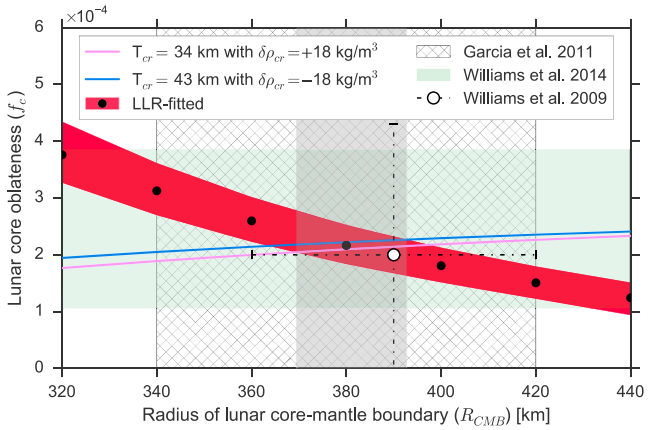

Figure 1. The lunar laser ranging (LLR)-fitted value of the lunar core oblateness f_c (in black dots with region of uncertainty in red) intersects the theoretical hydrostatic values of f_c (solid lines in violet and blue corresponding to models with two different lunar crustal thicknesses (34 and 43 km) with ±18 kg/m^3 crustal density variations, respectively) at a lunar CMB radius of $\mathcal{R}_{\rm CMB} = 381 \pm 12$ km (in gray region). The LLR-fitted mean values here are obtained by assuming a mean value of lunar crustal thickness ($T_{\rm cr} = (34+43)/2 = 38.5$ km) and density ($\rho_{\rm cr} = 2{,}550 \pm 18$ kg/m^3) estimates (Wieczorek et al., 2013) in the LLR dynamical model. A model with $T_{\rm cr} = 43$ km and $\delta\rho_{\rm cr} = -18$ kg/m^3 tends to increase the LLR-fitted mean value of f_c by 10.9 to 7.7%, while a $T_{\rm cr} = 34$ km and $\delta\rho_{\rm cr} = +18$ kg/m^3 tends to decrease the same by 10.7 to 8.5%, for $\mathcal{R}_{\rm CMB}$ varying from 320 to 440 km, respectively. The region of uncertainty of the LLR-fitted f_c (in red region) encompasses the cumulative errors from lunar core density (Garcia et al., 2011), crustal thickness and mean density variations (Wieczorek et al., 2013), degree-2 potential Love number (Konopliv et al., 2013), and other parameters listed in Table B2 in the order of decreasing precedence. Previously reported (Williams et al., 2009) f_c ($2.0 \pm 2.3 \times 10^{-4}$) is in agreement but with much larger error bars (in white dot). A more recent estimate (Williams et al., 2014) ($2.42 \pm 1.4 \times 10^{-4}$) covers plausible values of f_c obtained for $\mathcal{R}_{\rm CMB}$ ≈320 to 440 km (in green region). The estimated value of $\mathcal{R}_{\rm CMB} = 381 \pm 12$ km (in gray region) is obtained by the intersection of the lower and upper bounds of LLR-fitted f_c with the hydrostatic models of $T_{\rm cr} = 34$ and 43 km, respectively (see SI). The CMB radius agrees within 1σ of the Apollo seismic data analysis by Garcia et al. (2011) (in hatched region) and differs by 13% with Weber et al. (2011). Within these limits, the value of lunar core oblateness (f_c) is estimated as $(2.2 \pm 0.6) \times 10^{-4}$. In the figure, CMB refers to the core-mantle boundary.

bodies. They also describe the lunar orientation through Euler angles and state vectors, which are fitted to the reduced LLR observations (see Appendix). The combination of LLR observations with the lunar gravity field solutions derived from the Gravity Recovery and Interior Laboratory (GRAIL) mission (Konopliv et al., 2013; Lemoine et al., 2013) allows strong constraints to be placed on the dynamical model, enabling LLR to better resolve some correlated model parameters (Pavlov et al., 2016; Viswanathan et al., 2018; Williams et al., 2014). The "Intégrateur Numérique Planétaire de l'Observatoire de Paris" version 17a, abbreviated as INPOP17a (Viswanathan et al., 2018) allowed us to compare and validate our lunar dynamical model, LLR reduction procedure, and parameter adjustments against other analysis groups.

1.2. Context

The presence of a fluid core alters the angular momentum balance between the layers modeled through the Euler-Liouville equations for the total Moon (or the Moon),

$$\frac{\rm d}{{\rm d}t}(\mathcal{I}\Omega + \mathcal{I}_c\omega_c) + \Omega \times (\mathcal{I}\Omega + \mathcal{I}_c\omega_c) = \Gamma^{\rm external} \quad (1)$$

and for the fluid core,

$$\frac{\rm d}{{\rm d}t}\mathcal{I}_c(\Omega + \omega_c) + \Omega \times \mathcal{I}_c(\Omega + \omega_c) = \Gamma_c^{\rm friction} + \Gamma_c^{\rm inertial}. \quad (2)$$

Here, $\mathcal{I}$ is the moment of inertia (MoI) tensor for the Moon, ω is the angular velocity of the Moon, and $\Gamma^{\rm external}$ is the sum of the external torques acting on the Moon (i.e., figure-point mass interactions, figure-figure interactions, and de Sitter precession). The subscript "c" represents equivalent parameters for the core. We define ω_c as the angular velocity of the lunar core relative to that of the Moon. The lunar coordinate system is defined by the principal axes of the undistorted Moon, where the MoI tensor is diagonal. A set of Euler angles (ϕ, θ, ψ) defines the orientation of the principal axes frame to the inertial (ICRF2) frame. The MoI of the Moon varies with time due to tidal distortions from the Earth, Sun, and spin distortion (Viswanathan et al., 2018). The component of permanent tide is included within the tidal and spin distortions (Williams et al., 2001). The modeled dissipative torques arise from viscous friction due to differential rotation (Folkner et al., 2014) at the core-mantle boundary (CMB; $\Gamma_c^{\rm friction}$), while the inertial coupling torques (Rambaux et al., 2007) ($\Gamma_c^{\rm inertial}$) arise from the flow of the fluid along a nonspherical CMB.

The exchange of angular momentum between the layers forms the basis of sensitivity of LLR to the size and shape of the fluid core.

1.3. Motivation

LLR solutions are nonunique to a range of fluid core sizes (e.g., Figure A1) and this nonuniqueness primarily arises from model parameter correlations in the fit (see section 2). This study shows that the lunar core's hydrostatic nature (considering a nonhydrostatic lithosphere) can be used as an a priori to improve the previous constraints on the Apollo-seismic data-determined radius and LLR-observed geometry of the lunar CMB, both by a factor of 3 (see section 3). We show that this improvement allows a better determination of some derived quantities (e.g., lunar core mass fraction and lunar free core nutation) followed by concluding remarks on the future perspectives and applicability of this method to other planets.

2. Methodology

The LLR model is compatible with a range of fluid core sizes (Williams et al., 2014), often represented by the value of the ratio of the polar MoI of the lunar core to the total Moon ($\alpha_c = C_c/C_T$). The previous solution INPOP17a (Viswanathan et al., 2018) fixed α_c to a model value (7×10^{-4}), primarily due to its correlation

(Pearson correlation coefficient of −0.8) with the core oblateness f_c (where $f_c = [C_c - (\mathcal{A}_c + \mathcal{B}_c)/2]/C_c$ is used to describe the oblateness (also called polar flattening) of the core, through its principal components of the MoI tensor $\mathcal{A}_c$, $\mathcal{B}_c$, and C_c). While this allowed a close comparison to independent studies (Folkner et al., 2014; Pavlov et al., 2016), the previously reported (Viswanathan et al., 2018) uncertainty on f_c does not account for uncertainties from considering a fixed value for α_c. A different plausible model value of α_c (e.g., 3×10^{-4}) would increase the corresponding value of f_c by $\approx 2 \times 10^{-4}$, suggesting an uncertainty $\delta f_c \approx \frac{2\times10^{-4}}{\sqrt{2}} \approx \pm 1.4 \times 10^{-4}$ (see Williams et al., 2014). The uncertainty of f_c obtained thereof, encompasses the range of f_c obtained for a fluid core radii varying from ≈320 to 440 km (see Figure 1).

In a more direct approach, this study used the radius of the lunar CMB ($\mathcal{R}_{\mathrm{CMB}}$) as a model parameter, by redefining the principal components of the MoI of the core ($\mathcal{A}_c$, $\mathcal{B}_c$, and C_c). Other geophysical parameters involved in the MoI redefinition include the mean core density (ρ_c) and the CMB shape coefficients ($d_{nm,c}$, $e_{nm,c}$, where n and m are the degree and order, respectively) to represent a triaxial core, given by

$$\mathcal{I}_c = \frac{8\pi\rho_c\mathcal{R}_{\mathrm{CMB}}^5}{15\mathcal{M}\mathcal{R}_T^2}\begin{bmatrix} 1+\frac{1}{2}d_{20,c}-3d_{22,c} & -3e_{22,c} & -\frac{3}{2}d_{21,c} \\ -3e_{22,c} & 1+\frac{1}{2}d_{20,c}+3d_{22,c} & -\frac{3}{2}e_{21,c} \\ -\frac{3}{2}d_{21,c} & -\frac{3}{2}e_{21,c} & 1-d_{20,c} \end{bmatrix}. \quad (3)$$

The CMB polar shape coefficient ($d_{20,c}$) can be represented in terms of the core oblateness (f_c) using the integrals of the principal moments, given by $d_{20,c} = (-2/3)f_c$ (Meyer & Wisdom, 2011). This representation (Richard et al., 2014; equation 3) is convenient to explore plausible values of the MoI of the lunar core and place constraints on itself through a range of lunar interior models with varying core radii, densities, and surface shape coefficients. A set of equations based on this representation was implemented within INPOP, considering a lunar crust, mantle, and a triaxial fluid core. The triaxiality of the lunar core introduces additional components to the inertial coupling torque expansion (e.g., Rambaux et al., 2007) that impact the rotation of the Moon.

A reference lunar interior model is built from INPOP17a (Viswanathan et al., 2018) parameters and consists of three layers (crust, mantle, and fluid core) of constant density. For a given core radius, the reference (or hydrostatic CMB with nonhydrostatic lithosphere) model provides constraints on the core density and shape. The shape of the CMB for the reference model is calculated from a combination of the gravitational attraction of the crust, mantle, centrifugal acceleration, and mean tides (e.g., Dumberry & Wieczorek, 2016; Meyer & Wisdom, 2011; Wieczorek et al., 2019). A more detailed discussion on the reference model (e.g., Antonangeli et al., 2015; Chambat & Valette, 2008; Garcia et al., 2011; Matsuyama et al., 2016; Weber et al., 2011; Williams et al., 2014) can be found in the supporting information (SI). The gravity field of the Moon is constrained up to degree and order 6 from a GRAIL analysis (Konopliv et al., 2013). With the help of these constraints, an iterative least squares fit of the lunar dynamical model parameters to LLR data is performed. Each iterative fit started with initial values of geophysical parameters ($d_{20,c}$, $\mathcal{R}_{\mathrm{CMB}}$, and ρ_c) from the hydrostatic model. Subsequent iterations in the fit allowed for deviations of $d_{20,c}$ (the parameter of interest in this study) from the corresponding initial hydrostatic value. The fit of $d_{20,c}$ was necessary to maintain the recent (and most accurate) LLR postfit weighted root-mean-square to well-below 2 cm (see Figure A1). The value of the CMB equatorial shape coefficient ($d_{22,c}$) was held fixed to its hydrostatic value during the iterations, due to its insufficient sensitivity in the fit. Fits to LLR data show that the impact of varying the value of $d_{22,c}$ is indistinguishable at the present level of data accuracy. However, we still take into account a nonzero value of $d_{22,c}$ to quantify its impact on the estimation of $d_{20,c}$.

The off-diagonal elements of the MoI of the core (containing surface coefficients $d_{21,c}$, $e_{21,c}$, and $e_{22,c}$ in equation 3) are set to zero to align the principal moments of the lunar core with the principal axes of the undistorted Moon. Wieczorek et al. (2019) show possible deviations from this perfect alignment when a nonhydrostatic lithospheric model is considered, giving about 6.4° of tilt between the core principal polar moment with that of the Moon. We show that such a misalignment would introduce a relative error of below 1% on our core oblateness estimates (see SI).

3. Results and Discussions

The CMB polar shape coefficient ($d_{20,c}$) is fitted to LLR data over a range of previously expected CMB radii. Figure 1 shows this fitted value expressed in terms of the core oblateness (f_c) to allow comparisons with previous LLR estimates. The range of LLR-fitted (observed) values of f_c crosses its corresponding theoretical

hydrostatic values (obtained by considering variations in crustal thickness (34 and 43 km) and average density (2,550 ± 18 kg/m^3) from Wieczorek et al., 2013) at a CMB radius of 381 ± 12 km (highlighted region in gray). Within these limits, we obtain an estimated value of lunar core oblateness $f_c = (2.2 \pm 0.6) \times 10^{-4}$.

The intersection of the observed and theoretical values of f_c signifies that at the level of sensitivity of LLR data sets, the present-day lunar fluid core geometry satisfies the theoretical considerations of the case of a hydrostatic lunar fluid core within a nonhydrostatic lunar lithosphere. This is a suggested observational evidence in agreement with previous model predictions (Le Bars et al., 2011; Meyer & Wisdom, 2011). A recent study that used three-dimensional mantle convection models (Zhang et al., 2017) suggests the presence of a partially molten ilmenite-bearing cumulates (IBCs) rich layer with low viscosity surrounding the present-day lunar core. This offers additional explanation to the previously proposed low-viscosity, seismically attenuating layer near the CMB (Harada et al., 2016; Khan et al., 2014). With the viscosity at the base of the mantle $\eta_b \approx 10^{19}$ Pa s (a conservative value of overturned IBCs with 6 wt% ilmenite; Zhang et al., 2017), an approximate order of relaxation timescales of the CMB can be computed using the expression $\tau_r \sim \eta_b \mathcal{R}^2_{\mathrm{CMB}}/(\rho_c \Delta\rho \mathcal{G} \delta^3)$ (Nimmo et al., 2012). Here, η_b is the viscosity at the base of the lunar mantle (~10^{19} Pa s from Zhang et al., 2017), $\Delta\rho$ is the density contrast between the lunar core and mantle (~2,500 kg/m^3), and δ is the temperature and activation energy-dependent effective channel thickness (~21 km). With these conservative choice of values, we obtain CMB relaxation timescales of up to a few tens of million years (compared to the ~4.5 Gyr time since the formation of the Moon), supporting a present-day hydrostatic (or relaxed) core (Le Bars et al., 2011; Meyer & Wisdom, 2011) within a frozen-in nonhydrostatic lithosphere (e.g., Garrick-Bethell et al., 2014).

The region of error on the observed values of f_c was obtained after considering the impact of correlated parameters (fixed or constrained from previous analyses) in the fit (see Appendix). The largest contribution to the uncertainty on f_c (≤20%) arises from the uncertainty of the lunar fluid core density (between ≈5,000 and 7,000 kg/m^3) from the analysis of Apollo seismic data. The range of CMB radii shown in Figure 1 yield equally good fits of the lunar dynamical model to the LLR data used. This is evident from the variations of the weighted root-mean-square of LLR postfit residuals (see Figure A1), obtained after iterative fits of models with varying core radii, at an order of magnitude below the present-day LLR observational accuracy of about 5 mm (Courde et al., 2017; Murphy, 2013).

The mean value of the radius of the lunar CMB satisfying both the observed and the theoretical values of the core oblateness agree at a relative error of 0.3% with the Apollo seismic data analysis by Garcia et al. (2011) and differ by 13% with Weber et al. (2011). The improvement in the uncertainty with respect to Garcia et al. (2011) is by a factor of 3 to the hydrostatic case. Our estimates of CMB radii are in agreement with the analysis of Lunar Prospector spacecraft's magnetometer measurements (Hood et al., 1999).

The mass of the lunar core that corresponds to the estimated range of hydrostatic CMB radii lies between 1.59 and 1.77% of the total lunar mass $\mathcal{M}$ (where $\mathcal{M} \approx 7.346 \times 10^{22}$ kg is derived from joint lunar and planetary fits; Viswanathan et al., 2018). Previous estimates are in close agreement and lie between 1 and 3% (Hood et al., 1999) from Lunar Prospector (LP) mission, ≤1.5% (Williams et al., 2014) from GRAIL mission and 1.7–2.5% (Rai & van Westrenen, 2014) from the analysis based on siderophile element content in the lunar mantle. Simulations of moon-forming impact collisions (Canup & Asphaug, 2001) used upper limits on the previously estimated mass fraction (1–3%; Hood et al., 1999) of the present-day lunar core as a proxy for the mass fraction of iron in the orbiting equatorial disk mass (M_{Fe}/M_D), expected as a consequence of a giant impact on the proto-Earth. This enables the core mass fraction to constrain a range of head-on to off-axis collisions considered by such studies (Canup, 2012; Canup & Asphaug, 2001).

The Free Core Nutation (FCN) is a mode related to the nonalignment of the axis of rotation of the core and the mantle. The period of the FCN of the Moon (in days) is related to the core oblateness approximately as $\mathcal{P}_{\mathrm{FCN}} \approx 27.32/f_c$ (Rambaux & Williams, 2011). This gives a present-day $\mathcal{P}_{\mathrm{FCN}} \approx (367 \pm 100)$ years for the hydrostatic case, assuming a Poincaré flow within the lunar fluid core. The large value of $\mathcal{P}_{\mathrm{FCN}}$ with respect to the mantle precession (18.6 years) confirms that the present-day lunar core should be decoupled with the mantle (Meyer & Wisdom, 2011).

Tests of fundamental physics using LLR data rely on the accuracies of both the measurement and the model. Inaccurate size of the modeled lunar core introduces systematic biases in the tests of the principle of universality of free fall, estimated using parameter adjustments to LLR data (see a previous demonstration,

Williams et al., 2012). We validate the origin of such biases (of $\approx 4 \times 10^{-14}$ on the mean value of the fractional differential acceleration of the Earth and the Moon toward the Sun) by using plausible values of α_c. We obtain similar differences in solution values as given by Williams et al. (2012). Such biases are significant to LLR tests of the universality of free fall, since the current LLR detection limit is at the level of $\approx 7 \times 10^{-14}$ (Viswanathan et al., 2018).

4. Conclusions and Perspectives

This study compares the present-day lunar core oblateness obtained from LLR analysis with the expected hydrostatic model values, over a range of previously expected CMB radii. The findings suggest a core oblateness ($f_c = (2.2 \pm 0.6) \times 10^{-4}$) that satisfies the assumption of hydrostatic equilibrium over a tight range of lunar CMB radii ($\mathcal{R}_{\mathrm{CMB}} = 381 \pm 12$ km). This range of CMB radii agrees within one-σ of both seismological analysis (Garcia et al., 2011) and spacecraft magnetometer analysis (Hood et al., 1999). The accuracy of f_c and $\mathcal{R}_{\mathrm{CMB}}$ is improved by a factor of 3. Our estimates of a presently relaxed lunar CMB translates to a core mass fraction in the range of 1.59–1.77%, a parameter to limit the possible scenarios of giant impact during the formation of the Moon (Canup, 2012; Canup & Asphaug, 2001). The estimated core oblateness causes the present-day FCN of the Moon to be within (367 ± 100) years. Furthermore, an improvement in the knowledge of the lunar core radii allows a better understanding of the systematic biases in the solution values of LLR equivalence principle tests.

Future extension of the Apollo seismometer network with a better coverage (Mimoun et al., 2012) would allow a better determination of ρ_c and $\mathcal{R}_{\mathrm{CMB}}$ thereby improving current LLR estimations. With advancements in the LLR measurement (Adelberger et al., 2017; Courde et al., 2017) continuing to accumulate high-accuracy data sets and emerging observational techniques (Dehant et al., 2017), future LLR analysis will allow unprecedented access to the dynamical nature of the lunar interior. Moreover, the methods described here can be applied to study the influence of the liquid core on the rotation of other planets such as Mars (Folkner et al., 2018).

Appendix A: Lunar Interior Model Description

A.1. Dynamical Model

The dynamical equations within INPOP (Viswanathan et al., 2018) consider a uniform density lunar fluid core with its rotation resembling a rigid body and whose shape and size are constrained by the CMB. The

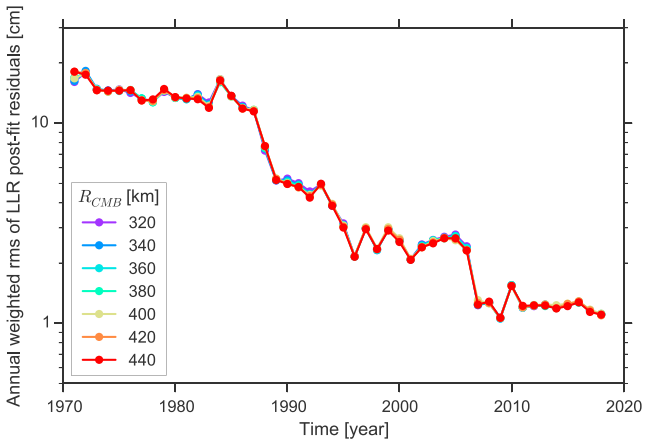

Figure A1. Annual weighted root-mean-square (wrms) of lunar laser ranging (LLR) postfit residuals obtained with the redefined dynamical model with the radius of the lunar core-mantle boundary ($\mathcal{R}_{\mathrm{CMB}}$) varying between 320 and 440 km at step sizes of 20 km. The variations in wrms of LLR postfit residuals between the solutions are well below the ≈5 mm observational accuracy of the LLR data set. The downward trend indicates an improvement in the observational accuracy of LLR data set by a factor of 20 over nearly five decades of observing. In the figure, CMB refers to the core-mantle boundary.

expression for the MoI of the undistorted total Moon can be expressed as

$$\mathcal{I}_T = \frac{\mathcal{C}_T}{\mathcal{M}\mathcal{R}_T^2}\begin{bmatrix}1&0&0\\0&1&0\\0&0&1\end{bmatrix} + \begin{bmatrix}C_{20,T}-2C_{22,T}&0&0\\0&C_{20,T}+2C_{22,T}&0\\0&0&0\end{bmatrix} \tag{A1}$$

where $C_{20,T}$ and $C_{22,T}$ are the unnormalized degree-2 Stokes coefficients for the spherical harmonic model of the undistorted Moon, and $\mathcal{C}_T/\mathcal{M}\mathcal{R}_T^2$ is the undistorted polar MoI of the Moon normalized by its mass $\mathcal{M}$ and radius squared $\mathcal{R}_T^2$. Through equation (A1), we can directly use the undistorted value of $C_{20,T}$ and $C_{22,T}$ from GRAIL-derived gravity field models (Konopliv et al., 2013).

The MoI matrix for a core ($\mathcal{I}_c$) can be represented using equation (3) where polar component $\mathcal{C}_c$ can be expressed equivalently in terms of lunar geophysical parameters as

$$\mathcal{C}_c = \alpha_c \mathcal{C}_T = \frac{8\pi}{15}.\frac{\rho_c \mathcal{R}_{\mathrm{CMB}}^5}{\mathcal{M}\mathcal{R}_T^2}.(1+\frac{2}{3}f_c) \tag{A2}$$

where $\mathcal{R}_{\mathrm{CMB}}$, ρ_c, $\mathcal{M}$ and $\mathcal{R}_T$ are the CMB radius, core density, the lunar mass, and lunar radius, respectively.

A.2. Hydrostatic CMB Model

A three-layer model of the Moon consisting of a lunar crust, mantle, and fluid core was considered. Using constraints of mass from a previous estimate (Viswanathan et al., 2018) and iteratively obtained MoI, the nonspherical deviations of each layer interface were estimated by limiting the nonhydrostaticity to the lunar crust (see SI).

Appendix B: Data Analysis and Regression

B.1. Data Processing

The processing (or reduction) of LLR data requires a precise light-time computation with accurate modeling of geophysical and relativistic effects, well described in previous studies (Petit & Luzum, 2010; Viswanathan et al., 2018). These refined reduction models enable a precise determination of the intrinsic distance information measured by the two-way time of flight of the laser pulses between one of the seven Earth stations and one of the five lunar retroreflectors. A reduction model for LLR data (Viswanathan et al., 2018) has been implemented within "Géodésie par Intégrations Numériques Simultanées," an orbit determination and processing software of the "Centre National d'Études Spatiales," validated through a step-wise comparative study.

B.2. LLR Fit

The fit of the lunar part of the ephemeris to LLR data involves solving for parameters linked to the Earth-Moon orbit and rotation. A full list of adjusted and fixed parameters relevant to the fit are provided in Table B1. CMB radii between 320 and 440 km with a step size of 20 km was chosen to be explored, with the interior model values listed in Table B3. For each CMB radius, the appropriate values of the density, shape, and radius were chosen from the lunar interior model (see SI), and an iterative fit to the LLR solution was performed. The solution parameters were adjusted according to a chosen type (fit, fixed or constrained) mentioned in Table B1, and the annual weighted root-mean-square of the postfit residuals are given in Figure A1.

B.3. Uncertainty of f_c

The formal uncertainties obtained from the least squares fit were too small to be considered realistic. Hence, the impact of correlated parameters that are fixed or constrained (e.g., ρ_c and $d_{22,c}$), on the estimates of core oblateness were tested. This includes analyzing the impact of variations (at known uncertainties) of these parameters on the solutions, to quantify the relative error introduced on f_c (see Table B2). A possible error from the nonlinear behavior of the partial derivatives of $\omega_{\mathbf{c}}$ is quantified using a two-step process:

1. Iterative fit of initial conditions of $\omega_{\mathbf{c}}$ with partial derivatives obtained with their initial conditions set to zero.
2. Fit of initial conditions of $\omega_{\mathbf{c}}$ with partials obtained with new initial conditions (nonzero values) obtained from previous step.

Table B1
Lunar Parameters Relevant to the Fit of the Dynamical and Reduction Model to LLR Observations

Parameter	Notation	Note
Lunar Euler angles and their rates	$\phi, \theta, \psi, \dot{\phi}, \dot{\theta}, \dot{\psi}$	initial condition (at J2000)
Core differential velocity	ω_c	initial condition (at J2000)
Geocentric position and velocity of the Moon	$\boldsymbol{r_{EM}}, \dot{\boldsymbol{r}}_{\boldsymbol{EM}}$	initial condition (at J2000)
Gravitational mass of E-M barycenter[a]	$\mathcal{GM}_{\mathrm{EMB}}$	INPOP17a (Viswanathan et al., 2018)
Earth-Moon mass ratio[a]	$EMRAT$	INPOP17a (Viswanathan et al., 2018)
Newtonian gravitational constant[a]	$\mathcal{G}$	CODATA: 2014 (Mohr et al., 2016)
Earth's orbital[a](O) and rotational (R) time delay	$\tau_{O(0,1,2)}, \tau_{R(1,2)}$	INPOP17a (Viswanathan et al., 2018)
Lunar time delay for solid-body tide	τ_M	—
Lunar gravity field (up to degree-6)	$C_{nm,T}, S_{nm,T}$	within GRAIL uncertainties (Konopliv et al., 2013)
	$C_{32,T}, S_{32,T}, C_{33,T}$	adjusted below 1% (Williams et al., 2014)
Lunar potential Love number	k_2	within GRAIL uncertainties (Konopliv et al., 2013)
Lunar vertical displacement Love number	h_2	—
Lunar horizontal displacement Love number[a]	l_2	model value of 0.0107 (Williams et al., 2014)
Polar MoI of the Moon	$C_T/\mathcal{M}\mathcal{R}_T^2$	Equation A1
Density of lunar core[a]	ρ_c	5,000 to 7,500 kg/m^3 (see SI)
Radius of core-mantle boundary[a]	$\mathcal{R}_{\mathrm{CMB}}$	320 to 440 km, 20 km steps
CMB polar shape coefficient	$d_{20,c}$	$f_c = -(3/2)d_{20,c}$ (Meyer & Wisdom, 2011) (see SI)
CMB equatorial shape coefficient[a]	$d_{22,c}$	hydrostatic value (see SI)
Euler angles for a nonprincipal axes CMB[a]	ν, ϵ, μ	Sensitivity test for non-zero off-diagonal core moments (see SI)
Coefficient of viscous friction at CMB	K_ν	—
Lunar retro-reflector (LRR) coordinates	$\boldsymbol{r}^{\mathrm{LRR}}_{x,y,z}$	5 LRR: A15, A14, A11, L1, L2
LLR station coordinates and velocities[a]	$\boldsymbol{r}^{sta}_{x,y,z}, \dot{\boldsymbol{r}}^{\mathrm{sta}}_{x,y,z}$	INPOP17a (Viswanathan et al., 2018)
LLR station biases	bias #	INPOP17a (Viswanathan et al., 2018)

Note. LLR = lunar laser ranging; CMB = core-mantle boundary.
[a]This represents fixed quantities.

The above steps were performed for two CMB radii (340 and 420 km). The solutions obtained between these two sets of partial derivatives impact the estimate of f_c at a relative error of 0.4%. The relative error introduced on f_c from a fixed value of lunar mass is expected to be below 0.2%, as the fractional uncertainty from the Newtonian gravitational constant ($\mathcal{G}$) is much larger than that from the lunar gravitational mass ($\mathcal{GM} = \mathcal{GM}_{\mathrm{EMB}}/(1 + \mathrm{EMRAT})$, where $\mathcal{GM}_{\mathrm{EMB}}$ is the gravitational mass of the Earth-Moon barycenter and EMRAT is the Earth-Moon mass ratio). The error on the estimated value of f_c (in Figure 1) results from

Table B2
Impact of Constrained Model Parameters on the Estimated Error on f_c at $\mathcal{R}_{CMB} \approx 381$ km

Parameter	Reference	Variation	Unit	Impact on f_c (rel. error %)
Core density (ρ_c)	Garcia et al. (2011)	±1000	kg/m^3	20
Crustal thickness (T_{cr})	Wieczorek et al. (2013)	34–43	km	6
Potential love number (k_2)	Konopliv et al. (2013)	$\pm 1.8 \times 10^{-4}$	1	3
Crustal density (ρ_{cr})	Wieczorek et al. (2013)	±18	kg/m^3	2
Tilt for a nonprincipal axes CMB (ϵ)	Wieczorek et al. (2019)	6.4	deg	1
CMB equatorial shape coefficient ($d_{22,c}$)	Reference model	$5 \times d_{22,c}$	1	0.5
Newtonian gravitational constant ($\mathcal{G}$)	Mohr et al. (2016)	$\pm 3.1 \times 10^{-15}$	m^3·kg^{-1}·s^{-2}	0.2
Mean lunar moment of inertia ($\overline{I}$)	Viswanathan et al. (2018)	$\pm 1 \times 10^{-5}$	1	0.1

*Note.*Relative error values provided are upper limits. The CMB equatorial shape was scaled up by a factor 5 of the reference model value following Le Bars et al. (2011). CMB = core-mantle boundary.

Table B3
Lunar Interior Model Values Obtained for $\mathcal{R}_{CMB}$ Varying Between 320 And 440 km in 20-km Step Size

$\mathcal{R}_{\mathrm{CMB}}$ (km)	ρ_c (kg/m^3)	α_c (10^{-4})	f_c (10^{-4})	$f_{c,(\mathrm{hydrostatic})}$ (10^{-4})	$C_T/\mathcal{M}\mathcal{R}_T^2$ (1)	K_v/C_T (10^{-9} rad/day)	τ_M (day)	h_2 (1)
320	7,621.4	4.92	3.76	1.85	0.39307	7.06	0.07534	0.04334
340	6,879.0	6.01	3.13	1.96	0.39311	7.32	0.07519	0.04333
360	6,288.4	7.31	2.60	2.07	0.39316	7.55	0.07503	0.04328
380	5,811.6	8.85	2.17	2.16	0.39322	7.72	0.07506	0.04332
400	5,421.6	10.66	1.81	2.24	0.39329	7.90	0.07484	0.04326
420	5,098.1	12.79	1.51	2.31	0.39338	8.02	0.07471	0.04336
440	4,826.7	15.28	1.24	2.37	0.39348	8.12	0.07489	0.04350

Note. CMB = core-mantle boundary.

the cumulative variations of the estimated values of f_c due to errors from fixed and constrained correlated parameters, tabulated in Table B2 in the order of decreasing precedence.

Acknowledgments
We acknowledge the ESEP (postdoctoral fellowship) and the PNGRAM for funding this research. The computations were performed on the servers of Geoazur-OCA and the LLR data processed using CNES-GRGS software (GINS). This work benefited from the previous contribution of H. Manche to the INPOP ephemeris development. We thank M. A. Wieczorek and two anonymous referees for their valuable comments that improved the manuscript. We acknowledge the continued efforts of personnel at Apache Point, Grasse, and older stations (Haleakala, Matera, and McDonald) for their respective contributions to the LLR data set, archived by the International Laser Ranging Service (Pearlman et al., 2002) at https://ilrs.cddis.eosdis.nasa.gov/data_and_products/data_centers/index.html

References

Adelberger, E. G., Battat, J. B. R., Birkmeier, K. J., Colmenares, N. R., Davis, R., Hoyle, C. D., et al. (2017). An absolute calibration system for millimeter-accuracy Apollo measurements. *Classical and Quantum Gravity*, *34*(24), 245008. https://doi.org/10.1088/1361-6382/aa953b

Antonangeli, D., Morard, G., Schmerr, N. C., Komabayashi, T., Krisch, M., Fiquet, G., & Fei, Y. (2015). Toward a mineral physics reference model for the Moon's core. *Proceedings of the National Academy of Sciences*, *112*(13), 3916–3919. https://doi.org/10.1073/pnas.1417490112

Bender, P. L., Currie, D. G., Poultney, S. K., Alley, C. O., Dicke, R. H., Wilkinson, D. T., et al. (1973). The lunar laser ranging experiment: Accurate ranges have given a large improvement in the lunar orbit and new selenophysical information. *Science*, *182*(4109), 229–238. https://doi.org/10.1126/science.182.4109.229

Canup, R. M. (2012). Forming a Moon with an Earth-like composition via a giant impact. *Science*, *338*(6110), 1052–1055. https://doi.org/10.1126/science.1226073

Canup, R. M., & Asphaug, E. (2001). Origin of the Moon in a giant impact near the end of the Earth's formation. *Nature*, *412*(6848), 708–712. https://doi.org/10.1038/35089010

Chambat, F., & Valette, B. (2008). A stress interpretation scheme applied to lunar gravity and topography data. *Journal of Geophysical Research*, *113*, 1–12. https://doi.org/10.1029/2007JE002936

Courde, C., Torre, J. M., Samain, E., Martinot-Lagarde, G., Aimar, M., Albanese, D., et al. (2017). Lunar laser ranging in infrared at the Grasse laser station. *Astronomy & Astrophysics*, *602*, A90. https://doi.org/10.1051/0004-6361/201628590

Dehant, V., Park, R., Dirkx, D., Iess, L., Neumann, G., Turyshev, S., & Van Hoolst, T. (2017). Survey of capabilities and applications of accurate clocks: directions for planetary science. *Space Science Reviews*, *212*(3-4), 1433–1451. https://doi.org/10.1007/s11214-017-0424-y

Dickey, J. O., Bender, P. L., Faller, J. E., Newhall, X. X., Ricklefs, R. L., Ries, J. G., et al. (1994). Lunar laser ranging: A continuing legacy of the Apollo program. *Science*, *265*(5171), 482–490. https://doi.org/10.1126/science.265.5171.482

Dumberry, M., & Wieczorek, M. A. (2016). The forced precession of the Moon's inner core. *Journal of Geophysical Research: Planets*, *121*, 1264–1292. https://doi.org/10.1002/2015JE004986

Folkner, W. M., Dehant, V., Le Maistre, S., Yseboodt, M., Rivoldini, A., Van Hoolst, T., et al. (2018). The rotation and interior structure experiment on the InSight mission to Mars. *Space Science Reviews*, *214*(5), 100. https://doi.org/10.1007/s11214-018-0530-5

Folkner, W. M., Williams, J. G., Boggs, D. H., Park, R. S., & Kuchynka, P. (2014). The planetary and lunar ephemerides DE430 and DE431. *Interplanetary Network Progress Report*, *196*, 1–81.

Garcia, R. F., Gagnepain-Beyneix, J., Chevrot, S., & Lognonné, P. (2011). Very preliminary reference Moon model. *Physics of the Earth and Planetary Interiors*, *188*(1-2), 96–113. https://doi.org/10.1016/j.pepi.2011.06.015

Garrick-Bethell, I., Perera, V., Nimmo, F., & Zuber, M. T. (2014). The tidal rotational shape of the Moon and evidence for polar wander. *Nature*, *512*(7513), 181–184. https://doi.org/10.1038/nature13639

Harada, Y., Goossens, S., Matsumoto, K., Yan, J., Ping, J., Noda, H., & Haruyama, J. (2016). The deep lunar interior with a low-viscosity zone: Revised constraints from recent geodetic parameters on the tidal response of the Moon. *Icarus*, *276*, 96–101. https://doi.org/10.1016/j.icarus.2016.04.021

Hood, L. L., Mitchell, D. L., Lin, R. P., Acuna, M. H., & Binder, A. B. (1999). Initial measurements of the lunar induced magnetic dipole moment using Lunar Prospector magnetometer data. *Geophysical Research Letters*, *26*(15), 2327–2330. https://doi.org/10.1029/1999GL900487

Khan, A., Connolly, J. A. D., Pommier, A., & Noir, J. (2014). Geophysical evidence for melt in the deep lunar interior and implications for lunar evolution. *Journal of Geophysical Research: Planets*, *119*, 2197–2221. https://doi.org/10.1002/2014JE004661

Konopliv, A. S., Park, R. S., Yuan, D.-N. N., Asmar, S. W., Watkins, M. M., Williams, J. G., et al. (2013). The JPL lunar gravity field to spherical harmonic degree 660 from the GRAIL primary mission. *Journal of Geophysical Research: Planets*, *118*, 1415–1434. https://doi.org/10.1002/jgre.20097

Le Bars, M., Wieczorek, M. A., Karatekin, Ö., Cébron, D., & Laneuville, M. (2011). An impact-driven dynamo for the early Moon. *Nature*, *479*(7372), 215–218. https://doi.org/10.1038/nature10565

Lemoine, F. G., Goossens, S., Sabaka, T. J., Nicholas, J. B., Mazarico, E., Rowlands, D. D., et al. (2013). High-degree gravity models from GRAIL primary mission data. *Journal of Geophysical Research: Planets*, *118*, 1676–1698. https://doi.org/10.1002/jgre.20118

Matsuyama, I., Nimmo, F., Keane, J. T., Chan, N. H., Taylor, G. J., Wieczorek, M. A., et al. (2016). GRAIL, LLR, and LOLA constraints on the interior structure of the Moon. *Geophysical Research Letters*, *43*, 8365–8375. https://doi.org/10.1002/2016GL069952

Meyer, J., & Wisdom, J. (2011). Precession of the lunar core. *Icarus*, *211*(1), 921–924. https://doi.org/10.1016/j.icarus.2010.09.016
Mimoun, D., Wieczorek, M. A., Alkalai, L., Banerdt, W. B., Baratoux, D., Bougeret, J.-L., et al. (2012). Farside explorer: Unique science from a mission to the farside of the Moon. *Experimental Astronomy*, *33*(2-3), 529–585. https://doi.org/10.1007/s10686-011-9252-3
Mohr, P. J., Newell, D. B., & Taylor, B. N. (2016). CODATA recommended values of the fundamental physical constants: 2014. *Reviews of Modern Physics*, *88*(3), 35009. https://doi.org/10.1103/RevModPhys.88.035009
Murphy, T. W. (2013). Lunar laser ranging: The millimeter challenge. *Reports on Progress in Physics*, *76*(7), 76901. https://doi.org/10.1088/0034-4885/76/7/076901
Nimmo, F., Faul, U. H., & Garnero, E. J. (2012). Dissipation at tidal and seismic frequencies in a melt-free Moon. *Journal of Geophysical Research*, *117*, E09005. https://doi.org/10.1029/2012JE004160
Pavlov, D. A., Williams, J. G., & Suvorkin, V. V. (2016). Determining parameters of Moon's orbital and rotational motion from LLR observations using GRAIL and IERS-recommended models. *Celestial Mechanics and Dynamical Astronomy*, *126*(1-3), 61–88. https://doi.org/10.1007/s10569-016-9712-1
Pearlman, M. R., Degnan, J. J., & Bosworth, J. M. (2002). The international laser ranging service. *Advances in Space Research*, *30*(2), 135–143. https://doi.org/10.1016/S0273-1177(02)00277-6
Petit, G., & Luzum, B. (2010). IERS conventions (2010). IERS Technical Note, 36, 179 http://iers-conventions.obspm.fr/2010officialinfo.php
Rai, N., & van Westrenen, W. (2014). Lunar core formation: New constraints from metal-silicate partitioning of siderophile elements. *Earth and Planetary Science Letters*, *388*, 343–352. https://doi.org/10.1016/j.epsl.2013.12.001
Rambaux, N., Van Hoolst, T., Dehant, V., & Bois, E. (2007). Inertial core-mantle coupling and libration of Mercury. *Astronomy and Astrophysics*, *468*(2), 711–719. https://doi.org/10.1051/0004-6361:20053974
Rambaux, N., & Williams, J. G. (2011). The Moon's physical librations and determination of their free modes. *Celestial Mechanics and Dynamical Astronomy*, *109*(1), 85–100. https://doi.org/10.1007/s10569-010-9314-2
Richard, A., Rambaux, N., & Charnay, B. (2014). Librational response of a deformed 3-layer Titan perturbed by non-Keplerian orbit and atmospheric couplings. *Planetary and Space Science*, *93-94*, 22–34. https://doi.org/10.1016/j.pss.2014.02.006
Viswanathan, V., Fienga, A., Minazzoli, O., Bernus, L., Laskar, J., & Gastineau, M. (2018). The new lunar ephemeris INPOP17a and its application to fundamental physics. *Monthly Notices of the Royal Astronomical Society*, *476*(2), 1877–1888. https://doi.org/10.1093/mnras/sty096
Weber, R. C., Lin, P.-Y., Garnero, E. J., Williams, Q., & Lognonne, P. (2011). Seismic detection of the lunar core. *Science*, *331*(6015), 309–312. https://doi.org/10.1126/science.1199375
Wieczorek, M. A., Beuthe, M., Rivoldini, A., & Van Hoolst, T. (2019). Hydrostatic interfaces in bodies with non-hydrostatic lithospheres. *Journal of Geophysical Research: Planets*, *124*, 1410–1432. https://doi.org/10.1029/2018JE005909
Wieczorek, M. A., Neumann, G. A., Nimmo, F., Kiefer, W. S., Taylor, G. J., Melosh, H. J., et al. (2013). The crust of the Moon as seen by GRAIL. *Science*, *339*(6120), 671–675. https://doi.org/10.1126/science.1231530
Williams, J. G., Boggs, D. H., & Ratcliff, J. T. (2009). A larger lunar core? In *Lunar and Planetary Science Conference*, *40*, Texas, pp. 1452. http://adsabs.harvard.edu/abs/2009LPI....40.1452W
Williams, J. G., Boggs, D. H., Yoder, C. F., Ratcliff, J. T., & Dickey, J. O. (2001). Lunar rotational dissipation in solid body and molten core. *Journal of Geophysical Research*, *106*(E11), 27,933–27,968. https://doi.org/10.1029/2000JE001396
Williams, J. G., Konopliv, A. S., Boggs, D. H., Park, R. S., Yuan, D. N., Lemoine, F. G., et al. (2014). Lunar interior properties from the GRAIL mission. *Journal of Geophysical Research: Planets*, *119*, 1546–1578. https://doi.org/10.1002/2013JE004559
Williams, J. G., Turyshev, S. G., & Boggs, D. H. (2012). Lunar laser ranging tests of the equivalence principle. *Classical and Quantum Gravity*, *29*(18), 184004. https://doi.org/10.1088/0264-9381/29/18/184004
Zhang, N., Dygert, N., Liang, Y., & Parmentier, E. M. (2017). The effect of ilmenite viscosity on the dynamics and evolution of an overturned lunar cumulate mantle. *Geophysical Research Letters*, *44*, 6543–6552. https://doi.org/10.1002/2017GL073702